epl A Letters Journal Exploring the Frontiers of Physics

July 2015

EPL, **111** (2015) 24002 www.epljournal.org
doi: 10.1209/0295-5075/111/24002

Non-universal Voronoi cell shapes in amorphous ellipsoid packs

Fabian M. Schaller[1,2(a)], Sebastian C. Kapfer[1,3], James E. Hilton[5], Paul W. Cleary[5], Klaus Mecke[1], Cristiano De Michele[6], Tanja Schilling[7], Mohammad Saadatfar[4], Matthias Schröter[2], Gary W. Delaney[5(b)] and Gerd E. Schröder-Turk[8,1,4(c)]

[1] *Institut für Theoretische Physik, Friedrich-Alexander-Universität Erlangen-Nürnberg - 91058, Erlangen, Germany*
[2] *Max Planck Institute for Dynamics and Self-Organization (MPIDS) - 37077 Goettingen, Germany*
[3] *Laboratoire de Physique Statistique, Ecole Normale Supérieure, UPMC, CNRS - 75231 Paris Cedex 05, France*
[4] *Applied Maths, RSPhysSE, The Australian National University, Canberra - Canberra, ACT 0200, Australia*
[5] *CSIRO Computational Informatics - Private Bag 33, Clayton South, Victoria, 3168, Australia*
[6] *Dipartimento di Fisica, "Sapienza" Università di Roma - P.le A. Moro 2, 00185 Roma, Italy*
[7] *Université de Luxembourg, Physics and Materials Research Unit - L-1511 Luxembourg, Luxemburg*
[8] *Murdoch University, School of Engineering & IT, Mathematics & Statistics - Murdoch, WA 6150, Australia*

received 13 April 2015; accepted in final form 9 July 2015
published online 4 August 2015

PACS 45.70.-n – Classical mechanics of discrete systems: Granular systems
PACS 61.43.-j – Disordered solids

Abstract – In particulate systems with short-range interactions, such as granular matter or simple fluids, local structure determines the macroscopic physical properties. We analyse local structure metrics derived from the Voronoi diagram of oblate ellipsoids, for various aspect ratios α and global packing fractions ϕ_g. We focus on jammed static configurations of frictional ellipsoids, obtained by tomographic imaging and by discrete element method simulations. The rescaled distribution of *local packing fractions* ϕ_l, defined as the ratio of particle volume and its Voronoi cell volume, is found to be independent of the particle aspect ratio, and coincide with results for sphere packs. By contrast, the typical *Voronoi cell shape*, quantified by the Minkowski tensor anisotropy index $\beta = \beta_0^{2,0}$, points towards a difference between random packings of spheres and those of oblate ellipsoids. While the average cell shape β of all cells with a given value of ϕ_l is similar in dense and loose jammed sphere packings, the structure of dense and loose ellipsoid packings differs substantially such that this does not hold true.

The universality of many features of disordered packings of spherical beads, with respect to preparation protocols and system parameters, is manifest in various properties, such as the universal value of the random close packing limit [1] and the universal distributions for contact numbers [2], free volumes [3,4] and Voronoi cell shape measures [3,5]. While ellipsoidal particles [6–14] and other aspherical particles [13–30] are receiving increasing attention, these questions of universality, including the independence of system parameters and preparation protocols, have not been comprehensively addressed yet. A qualitative difference between ellipsoid and sphere packings is revealed by the analysis of the Voronoi diagram of ellipsoid packings from various experimental and simulated origins.

(a) E-mail: fabian.schaller@physik.uni-erlangen.de
(b) E-mail: gary.delaney@csiro.au
(c) E-mail: g.schroeder-turk@murdoch.edu.au

Preparation protocols. – The experimental datasets (symbol □) comprise packings prepared by different protocols (fluidised beds, different funnels, grids, pouring particles, etc.) and compaction by vertical tapping. The ellipsoids have half-axes $a : c : c$ with $a \leq c$ and the aspect ratio is defined as $\alpha = a/c$. These datasets are the same as those used in ref. [31], comprising in total 73 datasets of jammed oblate ellipsoids of 5 different aspect ratios α and two different particle types (3D printed particles with $\alpha = 0.4, 0.6, 0.8, 1.0$ and considerable surface roughness; and sugar-coated pharmaceutical placebo pills with $\alpha = 0.59$ and lower friction coefficient μ, see table 1 and ref. [31]); the larger half-axis is $c = 3\,\text{mm}$ (smallest particles) to 4 mm (largest particles). The standard deviation of the particle volumes is 2–3%. The packings were imaged by X-ray tomography; image processing [32] was used to extract particle coordinates and orientations. The packings consisted of ≈5000 particles, of which 600–900

Table 1: Particle and packing properties.

Data set	Jammed	Gravity	Friction (μ)	Particles
□ Exp.	yes	yes	0.38–0.75	≈ 5000
▲ DEM	yes	yes	no	9323
⧫ DEM	yes	yes	0.01–1	9323
▼ DEM	yes	yes	1000	9323
○ MD	no	no	no	512
• MC	no	no	no	512
◐ ET	yes	no	no	1025

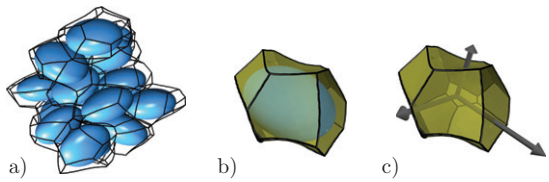

Fig. 1: (Color online) The Set Voronoi cells of ellipsoidal particles are, in general, non-convex with curved facets and edges. (a) Subset of an ellipsoid packing with Set Voronoi cells. (b) Single particle in its cell. (c) Principal axes (eigenvectors of $W_0^{2,0}$) of the cell.

were sufficiently far from cylinder walls to be included in the analysis; for the sake of spatial homogeneity, packings where radial variations of the packing fraction about the mean exceed 0.66% were discarded (as in ref. [31]). Data is available online [33].

We compare our experimental packings to 120 configurations obtained from discrete element simulations (DEM, [10]), of ellipsoids sedimenting into a square box in a viscous fluid under the action of gravity. Packings generated with a very high friction coefficient and viscosity constitute our estimate of the loosest possible packing (▼, sedimented loose packing, SLP, see discussion in [10]). Lower values of the friction coefficient and viscosity lead to denser packings (⧫). Frictionless particles lead to the highest packing fraction ϕ_g and give our estimate of the random close packing (RCP, ▲). The RCP estimate of the sedimented data is consistent with configurations obtained via a particle expansion method (ET, ◐) [15] and with earlier estimates of densest observed packings [6].

Reference data for equilibrium configurations of hard-core ellipsoids without gravity in the isotropic fluid phase (fig. 3) was obtained by event-driven molecular-dynamics simulations [34] (○, MD, the same data sets as in ref. [35]) and by canonical Monte Carlo simulations (•, MC, [36]).

Local structure metrics from the Set Voronoi diagram. – In the following, we adopt a local view, considering a particle and its immediate surroundings. We provide detailed data on the local geometry of packings, relevant for testing theoretical models such as the granocentric model [37] or other mean-field approaches [38]. For aspherical particles, the *Set Voronoi diagram* [39], also known as *navigation map* [40,41], provides a natural partition of space into N cells, each containing one of the N particles. The Voronoi cell of particle i is the compact set of points closer to particle i than to any other particle. The distance from a point in space to a particle is measured as the Euclidean distance to the nearest point on the bounding surface of the particle. This is in contrast to the conventional Voronoi diagram where the distance is measured with respect to the particle centre. Facets of the Set Voronoi diagram are in general curved and cells are non-convex, see fig. 1. For monodisperse spheres, the Set Voronoi diagram, henceforth simply referred to as the "Voronoi diagram", reduces to the conventional Voronoi diagram.

The local packing fraction of particle i is defined as $(\phi_1)_i = \nu_e/\nu_i$, where $\nu_e = 4\pi ac^2/3$ is the volume of the particle and ν_i the volume of the Voronoi cell K_i containing particle i. We characterise the shape of the Voronoi cell K_i by its volume moment tensor $W_0^{2,0} = \int_{K_i} \mathbf{x} \otimes \mathbf{x}\, \mathrm{d}v$, where $\mathbf{x}$ is the position vector relative to the center of mass $\mathbf{c}_i$ of K. Similar to the tensor of inertia, this tensor captures the distribution of mass; the notation $W_0^{2,0}$ derives from the theory of Minkowski tensors and integral geometry [42,43]. The three eigenvalues of this tensor are $\mu_i^{\min} \leq \mu_i^{\mathrm{mid}} \leq \mu_i^{\max}$. The ratio of minimal to maximal eigenvalue $\beta_i = \mu_i^{\min}/\mu_i^{\max} \in (0, 1]$ is an indicator of the shape anisotropy of the Voronoi cell K of particle i. Small values of β_i indicate elongated (anisotropic) cells. Note the difference to measures of asphericity [3] that quantify deviations from a spherical shape; the measure β_i is 1 (and K said to be *isotropic*) for any shape that has statistically identical mass distribution in any set of three orthogonal directions; this includes the sphere, but also regular polyhedra and the FCC, BCC and HCP Voronoi cells [44].

Probability distribution of Voronoi cell volumes. – The distribution of the Voronoi cell volumes of sphere packs has been studied in the context of granular materials [4,31,37,38], super-cooled liquids [3], and also with respect to granular entropy and the Edwards ensemble [45–53]. Aste *et al.* [4] have shown that in random jammed sphere packings below the RCP limit, the distribution of Voronoi volumes is universal and independent of the preparation protocol. Starr *et al.* [3] have obtained a similar result for super-cooled liquids. In both cases, the distributions of Voronoi cell volumes collapse when plotted as a function of $(\nu - \langle\nu\rangle)/\sigma$, where σ is the standard deviation of the distribution $P(\nu)$ and $\langle\nu\rangle$ its average. Aste *et al.* [4] proposed a derivation for a scaling $P((\nu - \nu_{\min})/(\langle\nu\rangle - \nu_{\min}))$, where $\nu_{\min}$ is the smallest possible Voronoi cell of equal-sized spheres and $\langle\nu\rangle = \sum_{i=1}^{N} \nu_i/N$ the average over all Voronoi cells.

Figure 2 demonstrates that this universality is not restricted to sphere packings, but holds more generally for jammed ellipsoid packings: To the resolution of our data, the functional form of the distribution depends neither on

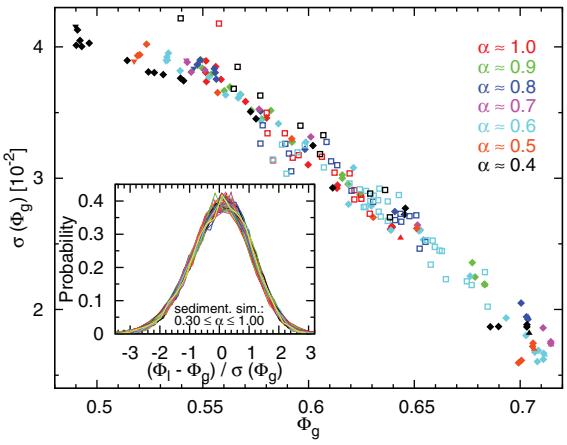

Fig. 2: (Color online) Collapse of the standard deviations of the local packing fraction distributions supports the universality of the probability distribution of the local packing fractions. The inset shows the probability distributions, comprising data sets between SLP and RCP with different aspect ratios $0.3 \leq \alpha \leq 1.0$ and friction coefficients $0 \leq \mu \leq 1000$.

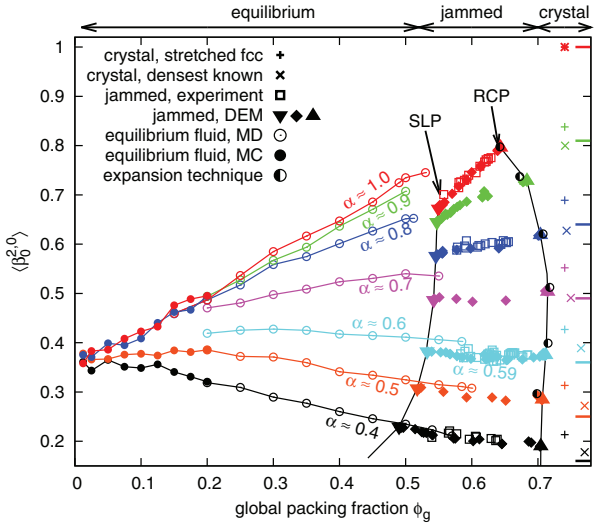

Fig. 3: (Color online) Average anisotropy $\langle\beta\rangle$ of the Set Voronoi cells of the ellipsoids as a function of ϕ_g for equilibrium ellipsoid configurations, static jammed ellipsoid and crystal packings. Dashes on the right-hand vertical axis mark the anisotropies of the particles themselves, *i.e.* β evaluated for a particle rather than its Voronoi cell. The vertical black lines represent the loosest (SLP) and densest (RCP) packings obtained by sedimented DEM simulations.

the global packing fraction ϕ_g nor on the particle aspect ratio α. The probability for a Voronoi cell in a jammed configuration with global packing fraction ϕ_g to have local packing fraction ϕ_l is written as $P(\phi_l \mid \phi_g)$. When plotted as $\sigma P(\phi_l \mid \phi_g)$ *vs.* $(\phi_l - \langle\phi_l\rangle)/\sigma$, it is invariant for all values of ϕ_g and α, see also ref. [31]. This plot shows good agreement between the experimental packings and jammed packings from simulations across the range of accessible packing fractions (those between SLP and RCP, see fig. 3) and aspect ratios $0.3 \leq \alpha \leq 1$. By contrast, data from equilibrium configurations does not rescale to the same curve.

The shape and anisotropy of the typical Voronoi cell (global averages). – Treating the Voronoi cell volume, or equivalently the local packing fraction ϕ_l, as the leading term of a shape description of the Voronoi cells, we now proceed to higher-order terms. While other scalar quantities, such as surface area, integrated curvatures or asphericities may contain signatures of such higher-order terms, we here use the tensorial shape measure $W_0^{2,0}$, similar to the tensor of inertia, and its eigenvalue ratio β to quantify the elongation of a cell.

Figure 3 shows the average Voronoi cell shape anisotropy, quantified by $\langle\beta\rangle = \sum_{i=1}^{N} \beta(K_i)/N$, as a function of global packing fraction ϕ_g. Data is for equilibrium ellipsoid fluids, experiments and simulations of jammed random ellipsoid packings and for two dense crystalline configurations (the *stretched fcc* obtained by scaling the x-coordinate of the fcc sphere packing, and the densest known structures discussed by Donev *et al.* [7]).

For equilibrium fluids in the limit of vanishing density $\phi_g \to 0$, where the typical distance between particles is large compared to the particle size, the Voronoi cell shape is independent of the particle shape. Consequently, the shape anisotropy corresponds to the value $\beta \approx 0.37$ of the Poisson point process [54]. For denser equilibrium fluids [35,36] the trend of the Voronoi shape anisotropy $\langle\beta\rangle$ can be understood by realising that the shape of the Voronoi cells approaches that of the particle itself when ϕ_g increases (see dashes on the right-hand vertical axis in fig. 3, evaluated for an ellipsoidal particle itself, rather than its Voronoi cell, the ratio is $\beta = (a/c)^2 = \alpha^2$, see appendix of ref. [42]). For small α, the curve $\langle\beta\rangle(\phi_g)$ hence decreases, while for larger α, $\langle\beta\rangle(\phi_g)$ increases with ϕ_g.

For the jammed packings, between SLP and RCP, our results for spheres ($\alpha = 1$) are in quantitative agreement with previously published data [5], with the cells becoming less elongated upon compaction, *i.e.* β increases with increasing ϕ_g. For ellipsoids with smaller value of α, the slope of $\beta(\phi_g)$ becomes smaller and eventually even adopts slightly negative values for small $\alpha < 0.60$. There is an excellent agreement between the experimental packings (□, with different preparation protocols) and the numerical data points from DEM simulations (▼, ♦, ▲). As previously found [42], sphere configurations exhibit a gap in shape anisotropy between the densest equilibrium configuration and the loosest jammed states. For ellipsoids, this discontinuity shrinks as the particle's aspect ratio decreases.

The shape and anisotropy of the typical Voronoi cell of a given size (local analysis). – The global packing fraction ϕ_g represents a useful parameter, easily accessible in experiments. However, there is no conceivable mechanism by which a locally defined quantity, such as

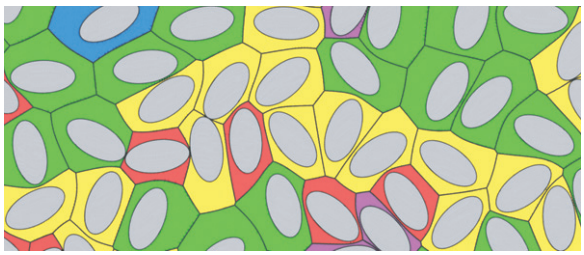

(a) Voronoi diagram with cells colored according to $(\phi_l)_i$

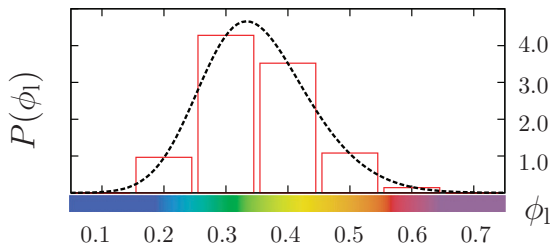

(b) Cell volume distribution $P(\phi_l) = P(\phi_l|\phi_g)$

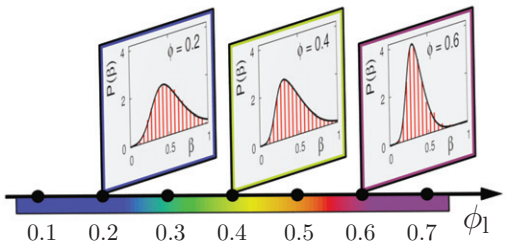

(c) Shape distributions $P(\beta) = P(\beta|\phi_l, \alpha, X)$

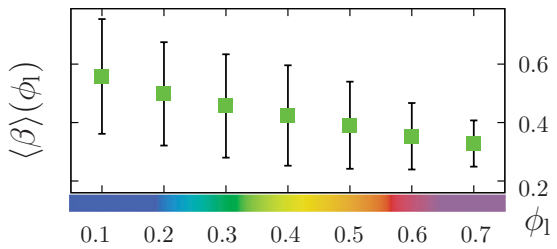

(d) Average shape parameter $\langle\beta\rangle(\phi_l)$

Fig. 4: (Color online) Illustration of the concept of the density-resolved local structure analysis, using an artificial two-dimensional system rather than the three-dimensional data in figs. 2, 3 and 5. Error bars in (d) represent the standard deviation of the distributions in (c). Note the choice of a large bin size (discretization) to help visual clarity; typical bin sizes for quantitative analyses are smaller.

the Voronoi cell shape or the contact number, can depend *directly* (*i.e.* by an immediate causal relation) on ϕ_g; a particle cannot sense the global packing fraction. That said, in packings with sufficient spatial homogeneity, correlations between averages of the local shape metrics and the global packing fraction are evidently possible, and commonly observed. Specifically, the study of the average contact number Z as a function of ϕ_g is a foundation of the jamming paradigm [31,55].

Here, we use a local density-resolved analysis based on the idea that the physical mechanisms underlying granular matter occur at the particle scale. This idea was applied to contact numbers in ref. [31] and is applied here to Voronoi cell shapes. Observed correlations between a *local* structure metric and the local packing fraction ϕ_l are hence more likely to yield physical insight than those with the *global* average ϕ_g. A similar approach has been used for the analysis of sphere packings [2,5].

Figure 4 illustrates the concept of the local density-resolved analysis. Particles are grouped by their local packing fraction $(\phi_l)_i$, *i.e.* into sets $\mathcal{S}(\phi_l)$ composed of all particles i with $\phi_l - \Delta/2 \leq (\phi_l)_i < \phi_l + \Delta/2$ for $\phi_l = \Delta, 2\Delta, 3\Delta, \ldots$ with a small interval Δ ($\Delta = 0.1$ in fig. 4, $\Delta = 0.02$ in fig. 5). We define the function $P(\beta \mid \phi_l, \alpha, X)$, which is the probability distribution of the shape measures β, restricted to the cells in $\mathcal{S}(\phi_l)$, *i.e.* to those with local packing fraction ϕ_l. The unknown parameters X capture influences from the packing protocol, friction, etc. As a result, the X may correlate with ϕ_g even though there need not be a causal dependence of the X on ϕ_g. The average $\langle\beta\rangle(\phi_l, \alpha, X) = \int \beta P(\beta \mid \phi_l, \alpha, X)\, \mathrm{d}\beta$ over all cells in $\mathcal{S}(\phi_l)$ provides information on how local structure changes depending on local packing fraction ϕ_l. In general, $\langle\beta\rangle$ also depends on the aspect ratio α and the unknown parameters X.

Figure 5 shows the result of this local structure analysis of β of jammed ellipsoid configurations. The key result is the following difference between sphere and ellipsoid packings: in sphere packings, the average shape of the Voronoi cells of a given local packing fraction ϕ_l is, as far as it is captured by the anisotropy index β, almost identical in dense and loose packings. This is evidenced by the near-collapse of the curves $\langle\beta\rangle(\phi_l, \alpha = 1, X)$ for packings of different global packing fraction. $\langle\beta\rangle$ is a function of ϕ_l only, but is largely independent of the unknown parameters X, the packing protocol and the particle friction.

In ellipsoid packings, illustrated for $\alpha = 0.8$ in fig. 5(a), the curves for different ϕ_g do not collapse. The average $\langle\beta\rangle(\phi_l, \alpha, X)$ depends on both α and X. This indicates that packings with low and high ϕ_g exhibit differences in their local structures controlled by α and X. Figure 5(b) demonstrates the validity of this result for other aspect ratios. Except for $\alpha = 1.0$ (spheres) and $\alpha \approx 0.6$ (close to the densest random ellipsoid packing), the local curves $\langle\beta\rangle(\phi_l)$ for the loosest and densest simulated packings do not collapse, which is indicative of structural differences.

Discussion and conclusion. – We have analysed the Voronoi diagram of oblate ellipsoid packings, establishing which aspects of the Voronoi diagram are universal, *i.e.* independent of preparation protocol and particle aspect ratio α and further parameters X, and which ones are not. Considering the geometric nature of this packing problem, these results have ramifications for our understanding of jammed systems and disordered solids.

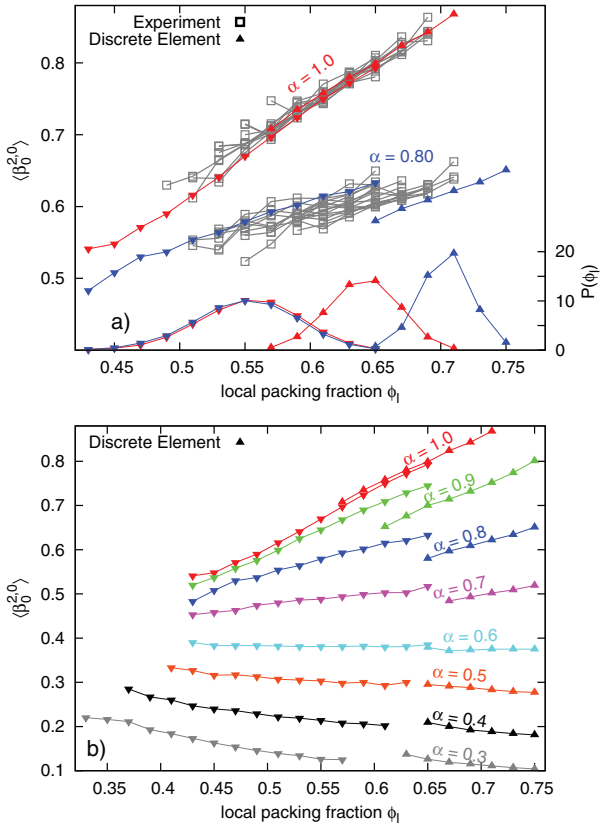

Fig. 5: (Color online) Relationship between local packing fraction ϕ_l and the Voronoi cell anisotropy β. Each curve represents a fixed value of ϕ_g, and is averaged over three independent realisations. (a) Local analysis for spheres ($\alpha = 1$) and slightly oblate ellipsoids ($\alpha = 0.8$). Gray symbols represent experimental configurations, for all available values of ϕ_g between RLP and RCP, and the red and blue curves show DEM simulations of SLP and RCP configurations. The curves on the bottom (using the right-hand abscissa) show the local packing fraction distributions $P(\phi_l)$ for each of the four simulated data sets. (b) Local Voronoi cell anisotropy $\langle\beta\rangle(\phi_l)$ for the DEM estimates for SLP and RCP packings for a larger range of aspect ratios.

The fact that ellipsoidal particles produce denser random packings than spheres is well established, with quantitative agreement between different studies of the value of the "random close packing" limit $\phi_{\mathrm{RCP}}(\alpha)$ as a function of the aspect ratio for oblate ellipsoids [6,10,15], see the curve labelled RCP in fig. 3. However, while a mean-field theory for $\phi_{\mathrm{RCP}}(\alpha)$ is developing [13], an intuitive geometric understanding for $\phi_{\mathrm{RCP}}(\alpha)$ is lacking. In this regard it is noteworthy that at $\alpha \approx 0.65$, the aspect ratio for which $\phi_{\mathrm{RCP}}(\alpha)$ is highest [6,10,15], the Voronoi cell shapes are found to be independent of the packing fraction. As far as captured by β of the volume moment tensor $W_0^{2,0}$, the shapes remain approximately constant for all jammed packings, both in the global (fig. 3) and in the density-resolved analysis (see the cyan $\alpha = 0.6$ curve in fig. 5(b)).

The results of fig. 5 emphasise an important distinction between random packings of spherical beads and those of aspherical beads. The structure of spherical bead packs is universal in the following sense: on average, the local structure of the typical particle of a given fixed but arbitrary local packing fraction ϕ_l is very similar in differently prepared packings, in particular with different ϕ_g. This observation, here made with respect to the Voronoi cell anisotropy of the volume moment tensor, is consistent with similar results for local contact numbers [2,31].

It implies that, at least with respect to averages of the volume tensor shape measure, the following interpretation of random jammed sphere packs is feasible. We consider a pool of local structure motifs for each value of the local packing fraction ϕ_l, given by the distributions in fig. 4(c). For spheres (but not for ellipsoids), these pools are universal in the sense that, for a fixed value of ϕ_l, the same pools can be used to construct packings of various global packing fractions ϕ_g. A jammed configuration can then be thought of as the composition of randomly drawn elements from the pools; the probability distribution $P(\phi_l)$ determines the fraction of cells to be drawn from each ϕ_l pool. While this clearly does not represent a constructive approach for the generation of disordered bead packs, it illustrates the universal nature of the sphere packing problem: the same pools of structural elements are used for all global packing fractions, just in different proportions. For ellipsoid packings, this universality breaks down and motifs in the ϕ_l pools depend on further parameters X and hence correlate with the global packing fraction.

We speculate that this geometric non-universality is paralleled by a significantly less universal nature of the random close packing problem in aspherical particles. More work is needed to identify the subtle origin of this non-universality. We have verified that it is neither solely an effect of particle orientation with the axis of gravity nor an obvious correlation with packing history. In particular the same non-universality is observed for two types of packings with different degrees of particle alignment with the axis of gravity (simulations and experiments).

Beyond these specific results for ellipsoidal particles, our analysis demonstrates the importance of the correct choice for the relevant parameters for the discussion of local structure metrics in granular matter. An analysis in terms of the local packing fraction ϕ_l, which may in principal *directly* relate to local physical processes, is more meaningful than the conventional analysis in terms of the global packing fraction ϕ_g.

* * *

We thank Weimer Pharma GmbH for the placebo pills, and Rolf Schilling for discussions. We acknowledge funding by the German Science Foundation through the research group "Geometry and Physics of Spatial Random Systems" under grant SCHR-1148/3-2. We thank Francesco Sciortino for the MD data.

REFERENCES

[1] Scott G. D., Knight K. R., Bernal J. D. and Mason J., *Nature*, **194** (1962) 956957.
[2] Aste T., Saadatfar M. and Senden T. J., *J. Stat. Mech.* (2006) P07010.
[3] Starr F. W., Sastry S., Douglas J. F. and Glotzer S. C., *Phys. Rev. Lett.*, **89** (2002) 125501.
[4] Aste T., Matteo T. D., Saadatfar M., Senden T. J., Schröter M. and Swinney H., *EPL*, **79** (2007) 24003.
[5] Schröder-Turk G. E., Mickel W., Schröter M., Delaney G. W., Saadatfar M., Senden T. J., Mecke K. and Aste T., *EPL*, **90** (2010) 34001.
[6] Donev A., Cisse I., Sachs D., Variano E. A., Stillinger F. H., Connelly R., Torquato S. and Chaikin P. M., *Science*, **303** (2004) 990.
[7] Donev A., Stillinger F. H., Chaikin P. M. and Torquato S., *Phys. Rev. Lett.*, **92** (2004) 255506.
[8] Baram R. M. and Lind P. G., *Phys. Rev. E*, **85** (2012) 041301.
[9] Xia C., Zhu K., Cao Y., Sun H., Kou B. and Wang Y., *Soft Matter*, **10** (2014) 990.
[10] Delaney G. W., Hilton J. E. and Cleary P. W., *Phys. Rev. E*, **83** (2011) 051305.
[11] Mailman M., Schreck C. F., O'Hern C. S. and Chakraborty B., *Phys. Rev. Lett.*, **102** (2009) 255501.
[12] Zeravcic Z., Xu N., Liu A. J., Nagel S. R. and van Saarloos W., *EPL*, **87** (2009) 26001.
[13] Baule Adrian, Mari Romain, Bo Lin, Portal Louis and Makse Hernán A., *Nat. Commun.*, **4** (2013) 2194.
[14] Wegner S., Stannarius R., Boese A., Rose G., Szabó B., Somfai E. and Börzsönyi T., *Soft Matter*, **10** (2014) 5157.
[15] Delaney G. W. and Cleary P. W., *EPL*, **89** (2010) 34002.
[16] Delaney G., Weaire D., Hutzler S. and Murphy S., *Philos. Mag. Lett.*, **85** (2005) 89.
[17] Williams S. R. and Philipse A. P., *Phys. Rev. E*, **67** (2003) 051301.
[18] Athanassiadis A. G., Miskin M. Z., Kaplan P., Rodenberg N., Lee S. H., Merritt J., Brown E., Amend J., Lipson H. and Jaeger H. M., *Soft Matter*, **10** (2014) 48.
[19] Baker J. and Kudrolli A., *Phys. Rev. E*, **82** (2010) 061304.
[20] Haji-Akbari A., Engel M., Keys A. S., Zheng X., Petschek R. G., Palffy-Muhoray P. and Glotzer S. C., *Nature*, **462** (2009) 773.
[21] Jaeger H. M., *Soft Matter*, **11** (2015) 12.
[22] Neudecker M., Ulrich S., Herminghaus S. and Schröter M., *Phys. Rev. Lett.*, **111** (2013) 028001.
[23] Smith K. C., Srivastava I., Fisher T. S. and Alam M., *Phys. Rev. E*, **89** (2014) 042203.
[24] Torquato S. and Jiao Y., *Nature*, **460** (2009) 876.
[25] Blouwolff J. and Fraden S., *Europhys. Lett.*, **76** (2006) 1095.
[26] Börzsönyi T., Szabó B., Törös G., Wegner S., Török J., Somfai E., Bien T. and Stannarius R., *Phys. Rev. Lett.*, **108** (2012) 228302.
[27] Fu Y., Xi Y., Cao Y. and Wang Y., *Phys. Rev. E*, **85** (2012) 051311.
[28] Kyrylyuk A. V., van de Haar M. A., Rossi L., Wouterse A. and Philipse A. P., *Soft Matter*, **7** (2011) 1671.
[29] Wouterse A., Luding S. and Philipse A. P., *Granular Matter*, **11** (2009) 169.
[30] Zhang Xiao-Dan, Xia Cheng-Jie, Xiao Xiang-Hui and Wang Yu-Jie, *Chin. Phys. B*, **23** (2014) 044501.
[31] Schaller F. M., Neudecker M., Saadatfar M., Delaney G. W., Schröder-Turk G. E. and Schröter M., *Phys. Rev. Lett.*, **114** (2015) 158001.
[32] Schaller F. M., Neudecker M., Saadatfar M., Delaney G., Mecke K., Schröder-Turk G. E. and Schröter M., *AIP Conf. Proc.*, **1542** (2013) 377.
[33] `http://dx.doi.org/10.5061/dryad.rf623`.
[34] De Michele C., *J. Comput. Phys.*, **229** (2010) 3276.
[35] De Michele C., Schilling R. and Sciortino F., *Phys. Rev. Lett.*, **98** (2007) 265702.
[36] Pfleiderer P., Milinkovic K. and Schilling T., *EPL*, **84** (2008) 16003.
[37] Newhall K. A., Jorjadze I., Vanden-Eijnden E. and Brujic J., *Soft Matter*, **7** (2011) 11518.
[38] Song C., Wang P. and Makse H. A., *Nature*, **453** (2008) 629.
[39] Schaller F. M., Kapfer S. C., Evans M. E., Hoffmann M. J., Aste T., Saadatfar M., Mecke K., Delaney G. W. and Schröder-Turk G. E., *Philos. Mag.*, **93** (2013) 3993.
[40] Luchnikov V., Medvedev N., Oger L. and Troadec J., *Phys. Rev. E*, **59** (1999) 7205.
[41] Luchnikov V., Gavrilova M., Medvedev N. and Voloshin V., *Future Gener. Comput. Syst.*, **18** (2002) 673.
[42] Schröder-Turk G. E., Mickel W., Kapfer S. C., Schaller F. M., Breidenbach B., Hug D. and Mecke K., *New J. Phys.*, **15** (2013) 083028.
[43] Mickel W., Kapfer S. C., Schröder-Turk G. E. and Mecke K., *J. Chem. Phys.*, **138** (2013) 044501.
[44] Kapfer S. C., Mickel W., Mecke K. and Schröder-Turk G. E., *Phys. Rev. E*, **85** (2012) 030301.
[45] Edwards S. F. and Oakeshott R. B. S., *Physica A*, **157** (1989) 1080.
[46] Anikeenko A. V., Medvedev N. N. and Aste T., *Phys. Rev. E*, **77** (2008) 031101.
[47] Zhao S.-C. and Schröter M., *Soft Matter*, **10** (2014) 4208.
[48] Pica Ciamarra M., Richard P., Schröter M. and Tighe B. P., *Soft Matter*, **8** (2012) 9731.
[49] Puckett J. G. and Daniels K. E., *Phys. Rev. Lett.*, **110** (2013) 058001.
[50] Paillusson F. and Frenkel D., *Phys. Rev. Lett.*, **109** (2012) 208001.
[51] Wu Y. and Teitel S., *Phys. Rev. E*, **91** (2015) 022207.
[52] Asenjo D., Paillusson F. and Frenkel D., *Phys. Rev. Lett.*, **112** (2014) 098002.
[53] Kumar V. S. and Kumaran V., *J. Chem. Phys.*, **123** (2005) 114501.
[54] Kapfer S. C., Mickel W., Schaller F. M., Spanner M., Goll C., Nogawa T., Ito N., Mecke K. and Schröder-Turk G. E., *J. Stat. Mech.* (2010) P11010. (Note that this reference uses the particle center as the origin for the analysis of $W_0^{2,0}$, rather than the center of mass of the Voronoi cell.)
[55] O'Hern C. S., Silbert L. E., Liu A. J. and Nagel S. R., *Phys. Rev. E*, **68** (2003) 011306.